Journal of Electron Spectroscopy and Related Phenomena 250 (2021) 147075

Contents lists available at ScienceDirect

Journal of Electron Spectroscopy and Related Phenomena

journal homepage: www.elsevier.com/locate/elspec

The CoESCA station at BESSY: Auger electron–photoelectron coincidences from surfaces demonstrated for Ag MNN

T. Leitner [a,b,*], A. Born [b,c], I. Bidermane [a,b], R. Ovsyannikov [a,b], F.O.L. Johansson [d], Y. Sassa [f], A. Föhlisch [a,b], A. Lindblad [a,d], F.O. Schumann [e], S. Svensson [a,d], N. Mårtensson [a,d]

[a] UBjL, Uppsala-Berlin joint Laboratory, Sweden, Germany
[b] Institute for Methods and Instrumentation in Synchrotron Radiation Research, Helmholtz-Zentrum Berlin für Materialien und Energie, Albert-Einstein-Strasse 15, 12489 Berlin, Germany
[c] Institut für Physik und Astronomie, Universität Potsdam, Karl-Liebknecht-Strasse 24-25, 14476 Potsdam, Germany
[d] Division Molecular and Condensed Matter Physics, Department of Physics and Astronomy, Uppsala University, Box 516, SE-751 20 Uppsala, Sweden
[e] Max-Planck-Institut für Mikrostrukturphysik, Weinberg 2, 06120 Halle, Germany
[f] Materials Physics, Chalmers University of Technology, SE-412 96 Gothenburg, Sweden

ARTICLE INFO

Keywords:
Auger
Photoelectron
Coincidence
Spectroscopy
AES
PES
APECS
Surface science

ABSTRACT

In this work, we present the CoESCA station for electron–electron coincidence spectroscopy from surfaces, built in a close collaboration between Uppsala University and Helmholtz-Zentrum Berlin at the BESSY II synchrotron facility in Berlin, Germany. We start with a detailed overview of previous work in the field of electron–electron coincidences, before we describe the CoESCA setup and its design parameters. The system is capable of recording shot-to-shot resolved 6D coincidence datasets, i.e. the kinetic energy and the two take off angles for both coincident electrons. The mathematics behind extracting and analysing these multi-dimensional coincidence datasets is introduced, with a focus on coincidence statistics, resulting in fundamental limits of the signal-to-noise ratio and its implications for acquisition times and the size of the raw data stream. The functionality of the CoESCA station is demonstrated for the example of Auger electron–photoelectron coincidences from silver surfaces for photoelectrons from the Ag 3d core levels and their corresponding MNN Auger electrons. The Auger spectra originating from the different core levels, $3d_{3/2}$ and $3d_{5/2}$ could be separated and further, the two-hole state energy distributions were determined for these Auger decay channels.

1. Introduction

After core electron photoionisation, an Auger process can occur, where the core hole is filled by an electron from a less bound shell, while a second electron is emitted, carrying the excess energy. A two-hole state is produced and two electrons linked to each other leave the sample, an Auger electron and a photoelectron. Since the initial vacancy state and the final two-hole state have well-defined energies for each element in the periodic table, the Auger electrons will be emitted with characteristic energies. In this way Auger Electron Spectroscopy (AES) can be used to identify which elements are present in a sample. Furthermore, for Auger transitions involving shallow core-levels, the Auger energies typically are in the range of a few hundred eV. For such electron energies the mean free path is relatively short and the Auger spectral information is surface sensitive. For this reason AES became a very powerful and much used tool in surface science.

One of the great successes of photoelectron spectroscopy is that one can perform detailed chemical analysis using the chemical shift. Also Auger transitions involving two core levels show chemical shifts. Due to the different, and often much larger chemical shifts, AES provides additional opportunities to distinguish different chemical species compared to photoelectron spectroscopy.

An important aspect of AES is that it provides information about the two-hole states of a system. For this reason it is well suited for probing electron correlation effects. In Core Valence Valence (CVV) Auger spectra from transition metals, the two final state holes may be delocalised, then the two-hole spectrum is a self-convolution of the single hole valence spectrum, just as measured by photoelectron spectroscopy. However, when electron correlation effects become more important towards the end of a transition series, localised final states start appearing, where the two final state holes are localised at the

* Corresponding author at: Institute for Methods and Instrumentation in Synchrotron Radiation Research, Helmholtz-Zentrum Berlin für Materialien und Energie, Albert-Einstein-Strasse 15, 12489 Berlin, Germany.
E-mail address: torsten.leitner@gmail.com (T. Leitner).

https://doi.org/10.1016/j.elspec.2021.147075
Received 17 December 2020; Received in revised form 8 April 2021; Accepted 7 May 2021
Available online 11 May 2021

same site. For late transition elements such as silver the spectrum is completely dominated by localised two-hole states.

There are a number of factors which often make the detailed analysis of Auger spectra complicated. All core levels are broadened due to their finite lifetime. The lifetime is typically in the range of a few fs and shorter. This leads to a broadening of the spectral features in the range of a few tenths of an eV up to a couple of eV for the transitions, which are most often used in Auger electron studies. In addition, also the two-hole final state has a finite lifetime. The lifetime broadening is more difficult to handle using fitting procedures for the Auger spectra than for photoelectron spectra. The two final state holes lead to multiplet effects and more complicated line shapes, which makes it more difficult to accurately parametrise the spectral profile. Often, there are also overlapping satellite transitions, due to multiple excited initial states caused by shake-up or shake-off processes in the creation of the initial vacancy. These multiple excited states may also be caused by the decay of deeper core hole states. These Auger satellites usually overlap the main spectral features, which severely complicates any detailed analysis.

One way to avoid these complications is to measure the Auger spectra in coincidence with the photoelectron spectra corresponding to the creation of the initial vacancy. This technique is usually denoted Auger PhotoElectron Coincidence Spectroscopy (APECS). There are a number of advantages of APECS, despite the fact that it involves quite demanding measurements. The key parameter is the ratio between true and accidental coincidences, which very much limits the useful count rates. The number of true coincidences will be proportional to the intensity of the exciting radiation I. The number of accidental coincidences will however scale as I^2. This sets a limit on what intensities are practical to use. The way to increase this ratio is to use spectrometers with the highest possible electron acceptance angle. For this reason there are still only relatively few examples of successful APECS measurements.

In a pioneering paper, Haak et al. [1] used APECS to disentangle the different components of the Cu $L_{23}M_{45}M_{45}$ Auger spectrum. They identified satellite lines in the $L_3M_{45}M_{45}$ part of the spectrum, caused by the $L_2M_{45}M_{45}$ Coster–Kronig (CK) process. Since then there have been a number of APECS measurements for the 3d transition elements. Thurgate and coworkers [2] have for instance investigated the transition from band-like final states in Fe and Co to localised final states in Ga.

One important property of APECS is that it enables the distinction of Auger spectra from different chemically shifted components of a system. The Auger spectra are quite broad and the differently shifted components usually overlap. However, by measuring the Auger spectrum in coincidence with chemically shifted, distinguishable, and often narrow, core-level peaks these spectra can be disentangled. In this way it has been possible to study Auger spectra from different sites at the reconstructed Si(111)7 × 7 surface [3,4]. Furthermore, the different stages of oxidation of this surface were also investigated [5].

One useful property of APECS, when studying solids, is that the coincident spectra are more surface sensitive than the photoelectron or Auger electron spectra. This is due to the fact that both the photoelectron and the Auger electron signals are attenuated due to the finite mean free path, which implies that the coincidence signal attenuates as a product of these effects. Using APECS it is furthermore possible to tune the surface sensitivity for the Auger spectra. The Auger electrons are measured in coincidence with the photoelectrons for which the kinetic energy and thereby also the mean free path can be varied by tuning the photon energy. Since the Auger electrons are measured in coincidence, they stem from the same depth.

When measuring Auger spectra in coincidence with the photoelectron spectra the uncertainty due to the finite lifetime can be removed. In such a case, an energy loss $-\Delta E$ for the photoelectron will by the conservation of energy lead to energy gain ΔE for the corresponding Auger electron. The only remaining lifetime broadening in the APECS spectra will hence be caused by the finite lifetime of the final states. This implies that one can study Auger processes and Auger two-hole final states which are not broadened by the lifetime of the core hole state. One advantage of this is that one is not restricted to using the narrowest core levels in order to achieve high resolution.

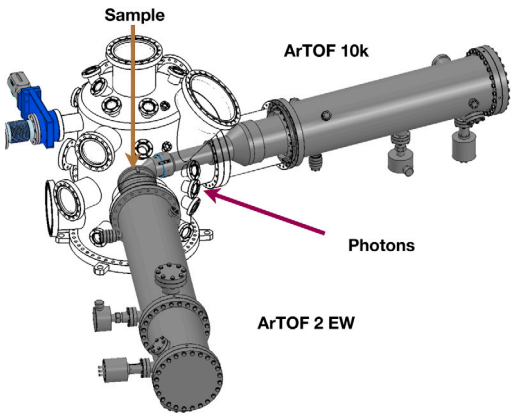

Fig. 1. Schematic of the CoESCA measurement setup. The X-rays enter the experiment from the right side in the figure and hit the sample in front of the spectrometers. The sample is not shown in this illustration. It is mounted on a 5-axis manipulator installed at the top flange of the analysis chamber.

In this connection the $N_{23}N_{45}N_{45}$ spectra in the 4d transition elements and the following elements up to Xe constitute a particularly interesting case. The Super Coster–Kronig character of the $N_{23}N_{45}N_{45}$ decay makes it very rapid and a one-step description of the excitation–deexcitation process becomes absolutely crucial. The distinction between the photoelectron and the Auger electron becomes less relevant and the shapes of the individual spectra may be heavily distorted [6]. However, by determining the sum of the energies of the emitted electrons with APECS, one can still accurately probe the energy spectrum of the $N_{45}N_{45}$ double-hole states, as demonstrated for Pd [7] and Ag [8].

One has also used coincidence techniques to probe the angular and energy correlation of a pair of electrons emitted from a surface upon impact of an electron of specific momentum [9] or excited by a beam of monochromatic photons [10]: In this way one has derived information on the exchange–correlation hole in solids.

In the present paper we describe the Coincidence Electron Spectroscopy for Chemical Analysis setup (CoESCA) at the BESSY II storage ring at HZB, Berlin. This system uses two high-resolution wide-angle time-of-flight ArTOF spectrometers. At first, we discuss how the coincidence measurements are done. Then we describe the CoESCA setup, and finally present some initial results.

2. Experimental setup

The Coincidence Electron Spectroscopy for Chemical Analysis (CoESCA) end-station is built at the BESSY UE52-PGM beamline which is a conventional soft X-ray plane-grating monochromator beamline, installed at an elliptical APPLE-II-type undulator, with a combination of a cylindrical and spherical mirror to provide a small horizontal focus of about 100 μm near the monochromator exit slit. The available photon energy is in the range from 120 eV up to 1600 eV and linear or elliptical polarisation can be set. The beamline offers a photon flux in the order of 10^{12} ph/s/100 mA and a resolving power of more than 10000 at 400 eV photon energy [11,12].

The CoESCA end-station is designed for electron–electron coincidence measurements on either in-situ or ex-situ prepared samples. It consists of an analysis chamber, equipped with two angle resolved time of flight (ArTOF) spectrometers [13], Fig. 1. The two ArTOFs are of different types reflecting the evolution of this type of spectrometers. One is an ArTOF 10k (actually the prototype) with an acceptance angle

of ±14° and the other instrument is an ArTOF 2 EW type with a wide acceptance angle of ±24°. Both spectrometers are positioned at a 54.6° angle with respect to the incoming photon beam.

The sample is placed on a 5-axis manipulator (xyz-position, polar- and azimuthal rotations) with active sample heating or cooling in a temperature range from 30 K up to 900 K. A radial sample transfer system connects the analysis chamber with a load lock for sample introduction, a sample storage and a sample preparation chamber. The preparation chamber is equipped with a 4-axis manipulator with resistive heating, direct current heating or electron bombardment options (up to 1200 K) and provides sample current and temperature, a sputter gun and a quartz balance. There are a number of free ports for further equipment like evaporators or gas dosing systems. Another utility chamber (not shown in Fig. 1) is situated on top of the analysis chamber, and is equipped with mass spectrometer, sputter gun and extra flanges for more user equipment. In addition, there are free access ports to our sample transfer system for accommodating user provided chambers to carry out specific sample preparations.

The ArTOF electron spectrometers use advanced electron lenses in combination with measuring the time-of-flight of the electron and its impact position on the detector at the end of the flight tube. From this, the exact particle trajectory through the lens system can be calculated including the take-off angle of the electron providing for full 3d electron distributions in "one shot", i.e. for one set of parameters for electron analyser, beamline and sample position. The kinetic energy is determined from the time-of-flight and the precisely known length of the flight path [13]. The instruments can, of course, be operated in non-coincidence mode for advanced studies of materials where, for example, two different core level regions can be monitored simultaneously while scanning an experimental parameter, such as the sample temperature.

ArTOF spectrometers demand a pulsed light source with a minimum time separation between the pulses, which depends on the chosen electrostatic lens mode and the kinetic energy of the electrons under investigation. For ArTOF measurements at the UE52-PGM beamline, the pulse-picking-by-resonant-excitation (PPRE) mode of BESSY II is used, providing quasi single bunch pulses separated by 800 ns (repetition rate of 1.25 MHz) [14].

3. Measuring coincidences

In our setup an event is stored as a coincidence, if one electron is detected in each spectrometer after excitation by the same photon pulse. The data is 7-dimensional: 3D for each electron (x,y-hit coordinates and arrival time coordinate t) stored together with a trigger timestamp:

$$\text{Event} = \{x_1, y_1, t_1, x_2, y_2, t_2, trig\}. \quad (1)$$

True coincidences are pairs of electrons which are created by absorption of one photon. However, there is also a background of accidental coincidences. In this case, the two detected electrons have been excited by the same photon pulse, but they originate from two different photons, hence different sites in the sample. The aim is to measure the true coincidence distribution as accurately as possible and in the shortest possible time. There is no way experimentally to directly distinguish true from accidental coincidences. However, one can instead separately determine the distribution of only accidental coincidences and subtract them to derive the distribution of true coincidences from the data. It is then essential that the distribution of accidental coincidences is measured in exactly the same way as the full coincidence distribution.

Our setup is ideally suited for achieving this. During the experiment, a database is written containing each event in each detector together with a timestamp, which serves as a unique photon pulse ID. In post-processing, true & accidental coincidences measured from the same pulse (all coincidences) are extracted from the data, for events where an electron was detected in both detectors for the same pulse. Accidental coincidences are extracted for cases, where one electron is recorded in each spectrometer, but for events from two different photon pulses (accidental coincidences).

The data lists are sorted into multi-dimensional histogram distribution matrices M. The distribution for coincidences from one photon and one site in the sample, the true coincidences dataset M_t, is derived in post-processing by a simple subtraction of the accidental distribution M_a from the all coincidences distribution M_c:

$$M_t = M_c - M_a \quad (2)$$

with

$$M_a = \frac{1}{\gamma} M_\gamma, \quad (3)$$

where γ is the number of virtual pulses per real pulse, which are analysed for accidental coincidences to get the measured distribution of accidentals M_γ. In our case, the accidental data is created from comparing *detector A, pulse N* with *detector B, pulse N-1* and, vice versa, from comparing *detector A, pulse N-1* with *detector B, pulse N*. Hence, it is created from twice as many virtual pulses than the all coincidences map and therefore $\gamma = 2$.

The full 6D coordinates can be used to analyse the data. In most cases one looks at 2D maps of E_1 vs. E_2 (see Figs. 3 and 4), but any other combination of coordinates can be used, for example one can additionally discriminate by the angles of the electrons and look at coincidences resolved in energy- and k-space.

All events are stored in a list-like database together with a timestamp. This enables a variety of possibilities for post treatment and analysis of the data. One may for instance detect, that there have been some changes of the sample during the measurements due to contamination or radiation damage and that therefore only a subset of the collected data is useable. This can be based on a careful analysis of the singles spectra, extracted from the data base. The singles spectra are calculated by evaluating the signals for each ArTOF independently, without looking for coincidences. This yields the same spectra as in a classic non-coincident setup. These spectra are very useful, since they usually have two to three orders of magnitude higher count rates than the coincidence data. If a subset is identified in the singles data, where the changes can be neglected, one knows that the corresponding subset can be used also for the coincidence data. Furthermore, when using only part of the coincidence data this can always be connected to the corresponding determination of the accidental coincidences. All these spectra have in this case been recorded under exactly identical conditions.

The fact that the events are stored together with a timestamp, makes the experiment well adapted to studies of time-dependent phenomena. One can study slow processes, where the theoretical time resolution is set by the separation of the X-ray pulses, which in the case of BESSY II in the single bunch mode is 800 ns. In praxis, this time resolution is much slower and governed by the data statistics, since the low count rates make it necessary to integrate over many X-ray pulses before enough useful information can be found in the data set.

An Auger spectrum provides information on the energies of two-hole states of a system. Usually, the two-hole energies are determined from an Auger spectrum by subtracting the core level binding energy from the Auger energies. By doing so, the Auger spectrum is plotted on an energy scale which corresponds to the binding energy for the two-hole final states, but the spectrum will be influenced by any broadening effect connected to the core ionisation. On the other hand, in a coincidence measurement it is possible to derive the binding energy of the two-hole final state directly. The energies of the photoelectron and the Auger electron are both measured for each coincident event. The two-hole energy is then obtained by subtracting the sum of both electron energies from the photon energy. In our set-up it is straight-forward to extract the two-hole energy spectrum it can be derived directly from the true coincidence map by summing the kinetic energies for each point in the map. The two-hole spectrum, derived in this way, is not broadened by the core-hole life time, which is a great advantage since this extends the range of core levels which can be used for detailed measurements.

Effective coincidence count rate and limitations

The true and accidental coincidence count rates are small compared to the primary particle pulse repetition rate. For example, at CoESCA we typically see an order of 10^{-6} coincidence counts per photon pulse. The measured signals from different pulses are pair-wise independent and do not influence each other. Therefore, we can describe the behaviour of the probability of k events detected for the same pulse for an average rate of events per pulse λ with a Poisson distribution:

$$P_\lambda(k) = \frac{\lambda^k}{k!} e^{-\lambda} \overset{(\lambda \ll 1)}{\approx} \frac{\lambda^k}{k!} \tag{4}$$

λ scales linearly with the incident flux, i.e. the number of primary particles per pulse (e.g. photons). In [15], Jensen et al. provide a detailed analysis of the link between electron count rates and experimental parameters, such as primary particle flux, total detection volume, detection efficiencies and cross-sections for electron pair creation.

For a true coincidence, one primary particle is absorbed ($k = 1$), which creates one electron pair, leading to one coincidence event in the detectors. An accidental coincidence occurs, when two primary particles are absorbed in the sample ($k = 2$), and two electrons, which are recorded by the detectors, are created at two different sites. Events for more than two absorbed primary particles can be neglected, since the probability drops very fast with ($\lambda^k/k!$). The probabilities for detecting a true ($k = 1$) or accidental ($k = 2$) coincidence read as:

$$\begin{aligned} P_\lambda(1) &\approx \lambda, \\ P_\lambda(2) &\approx \frac{1}{2}\lambda^2. \end{aligned} \tag{5}$$

The probability of finding any number of events for a single pulse is the sum over $P_\lambda(k)$ for all k. And the probabilities for any two distinct pulses $A\&B$ are linearly independent. Thus, the probability to record an accidental coincidence from these two pulses is the product of the probabilities of measuring one or more events from each pulse independently:

$$\begin{aligned} P_\lambda^{A\&B} = P_\lambda^A \, P_\lambda^B &= \left[\sum_{k>0} P_\lambda(k)\right]^2 \\ &\approx \left[P_\lambda(1)\right]^2 = \lambda^2 = 2\, P_\lambda(2) \end{aligned} \tag{6}$$

The equation above states, that the accidental coincidence signal, which is derived from comparing pairs of different pulses is twice as intense as the accidental contribution to the coincidences signal derived from single pulses only. This is accounted for in Eq. (3) by the scaling factor $\frac{1}{\gamma}$.

The true and accidental count rates are defined as counts per time. They are linearly proportional to the respective $P_\lambda(k)$. However, the proportionality constants are different for measuring true or accidental coincidences, since the detection volume for accidental coincidences is larger than for true coincidences, and since there is a contribution to the accidental coincidences arising from competing events against which one is trying to discriminate, like for example inelastic scattering of higher energy electrons [15]. In order to respect these proportionalities, constants are introduced, which connect the count rates ν_t, ν_a with the respective probabilities $P_\lambda(k)$:

$$\begin{aligned} \nu_t &= \sigma_t \; P_\lambda(1) \propto \lambda, \\ \nu_a &= \sigma_a \, P_\lambda(2) \propto \lambda^2. \end{aligned} \tag{7}$$

The rate of all coincidence counts per time, measured from single pulses is given by the sum of the true and accidental coincidence count rates:

$$\nu_c = \nu_t + \nu_a. \tag{8}$$

For a given acquisition time τ, the number of all coincidence counts measured in an experiment is $N_c = \nu_c \, \tau$ and the number of accidental counts in this signal is $N_a = \nu_a \, \tau$. The ratio of these counts can be expressed as:

$$R = \frac{N_c}{N_a} = \frac{\nu_t + \nu_a}{\nu_a} \propto \lambda^{-1} + 1 \tag{9}$$

and it approaches $R = 1$ for an infinite flux of primary particles λ.

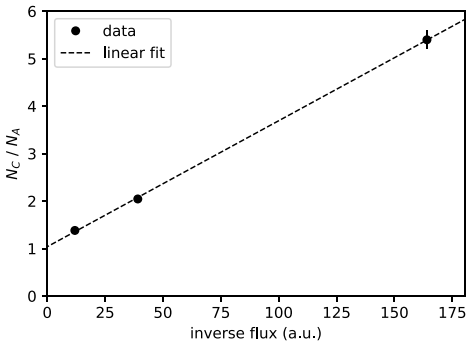

Fig. 2. Ratio R of coincidence counts from one pulse N_{coin} and coincidence counts from two pulses N_{acc} versus the inverse flux. The fitted line extrapolates to $R_0 = 1.038 \pm 0.001$ for an inverse flux of 0, which confirms the validity of our assumptions in Eqs. (4)–(9).

In order to validate the assumptions and approximations in Eqs. (4)–(9) for our setup, we performed short coincidence runs for three different light intensities and determined N_c and N_a for each run. Fig. 2 shows the ratios R from these runs versus the inverse flux, which was deduced from the singles count rates. A linear fit extrapolates $R_0 = 1.038 \pm 0.001$ for $\lambda^{-1} = 0$, which is in good agreement with the theoretical value of 1 and validates our assumptions.

The ratio of accidental to true counts for events recorded from single pulses is an important parameter for coincidence experiments. From Eq. (7) we see that this ratio is given by:

$$\nu_a/\nu_t \propto \lambda \propto \text{flux}. \tag{10}$$

The higher the flux, the higher the relative accidental background, therefore simply increasing the flux is not beneficial for a coincidence experiment. On the other hand, simply lowering the intensity in order to remove almost all accidental coincidences leads to low count rates and therefore long acquisition times. In order to judge the flux and the acquisition time needed to achieve a dataset of acceptable quality, it is useful to look at the behaviour of the ratio of the derived true coincidences signal and its statistical error, i.e. the signal-to-noise ratio S of the true coincidences dataset as calculated from the measured data:

$$S = M_t/\Delta M_t \tag{11}$$

This ratio can be interpreted as the amount of useful information, which is added to the data for a given acquisition time. In [15], the authors discuss the conditions for reaching a certain value of this ratio in a coincidence measurement, starting from very basic assumptions. In their considerations, the contributions to the statistical noise, which originate from the subtraction for calculating the true coincidences in Eq. (2) are approximated as negligible. They find, that the signal-to-noise ratio approaches an asymptote, when the flux of primary particles becomes too high. Here, we present a calculation of S, which is adapted to our data acquisition system and includes all contributions to the statistical error of the derived true coincidences dataset, which arise from the measurements of all coincidences from single pulses, M_c, and the determination of the accidental coincidences M_a from comparing pairs of different pulses. These two datasets and their statistical noise can be defined in terms of the count rates ν_t and ν_a and the acquisition time τ. Please note, that the following considerations, about the statistical quality of the counts in our multidimensional data matrices M_x apply to each single point within the matrices. Therefore, they also apply to

the sum of a subset of these matrices, when binning the data. The total count rates $N_x = \sum M_x$ are the extreme case of binning to one single point per dataset.

The coincidences originating from single pulses, M_c, are measured directly and can be described as:

$$\begin{aligned} M_c &= (\nu_t + \nu_a)\tau \\ \Delta M_c &= \sqrt{M_c} = \sqrt{(\nu_t + \nu_a)\tau} \end{aligned} \tag{12}$$

The accidental dataset M_a is derived from M_γ, which was measured with a statistical error of $\Delta M_\gamma = \sqrt{M_\gamma}$, we get:

$$\begin{aligned} M_a &= \tfrac{1}{\gamma} M_\gamma = \nu_a \tau \\ \Delta M_a &= \tfrac{1}{\gamma}\sqrt{M_\gamma} = \sqrt{\nu_a \tau/\gamma} \end{aligned} \tag{13}$$

The true dataset M_t and its statistical error can be written as:

$$\begin{aligned} M_t &= M_c - M_a = \nu_t \tau \\ \Delta M_t &= \sqrt{(\Delta M_c)^2 + (\Delta M_a)^2} \\ &= \sqrt{\left(\nu_t + (1+\tfrac{1}{\gamma})\nu_a\right)\tau}. \end{aligned} \tag{14}$$

Hence, with $\nu_t \propto \lambda$ and $\nu_a \propto \lambda^2$, see Eq. (7), we get:

$$\begin{aligned} S &= \sqrt{\frac{\tau}{\nu_t^{-1} + (1+\tfrac{1}{\gamma})\nu_a \nu_t^{-2}}} \\ &\propto \sqrt{\frac{\tau}{\lambda^{-1} + 1 + \tfrac{1}{\gamma}}} \end{aligned} \tag{15}$$

From Eq. (15), we see that the signal-to-noise ratio, S, approaches an asymptote for infinite flux. A closer analysis discloses, that the gain in signal quality decreases rapidly already for increasing the flux above a level corresponding to an accidental to true ratio of $\nu_a/\nu_t = 1$. Hence, the acquisition time, which is necessary to achieve a desired statistical quality of the true coincidence data does not substantially decrease anymore for going to higher fluxes. On the other hand, a further increase of the flux quadratically increases the number of recorded events and hence the amount of data to be stored. For example, at $\nu_a/\nu_t = 10$, depending on the sample, the CoESCA station can easily produce more than 500 GB of coincidence data for a typical measurement week of 6×12-hour shifts. This corresponds to two or three coincidence maps, i.e. combinations of Auger and Photoelectron energy window settings of the detectors.

In order to increase S, a data analysis scheme for working with $\gamma > 2$ is currently being developed for the CoESCA station. The accidentals dataset M_γ will be created by adding up the accidentals analysis results from pulse pairs (N,N-1), (N,N-2), … , (N,N-K), with $K = \gamma/2$. The theoretical limit of S for $\gamma \to \infty$ corresponds to the intrinsic signal-to-noise ratio arising from the measurement of the coincidence signal only and equals to $M_t/\Delta M_c$.

The best way to strongly reduce acquisition times, while remaining at an acceptable data rate is to increase the number of experiments per time, hence the pulse repetition rate. However, in this experiment the pulse repetition rate from the storage ring was fixed to 1.25 MHz.

4. Results & discussion

Arena et al. have previously reported Ag 3d-M_{45}NN APECS measurements [16] and shown how coincidence spectroscopy can be used to determine the intrinsic shapes of overlapping spectral lines. In their experiment, they measured the coincidences with two cylindrical mirror electron analysers (CMA) of 1 eV instrumental resolution. One CMA was set to a fixed energy in the Auger region, while the second CMA scanned the core level spectrum and, vice versa, one CMA was set to a fixed core level energy region, while the other CMA scanned the Auger spectrum.

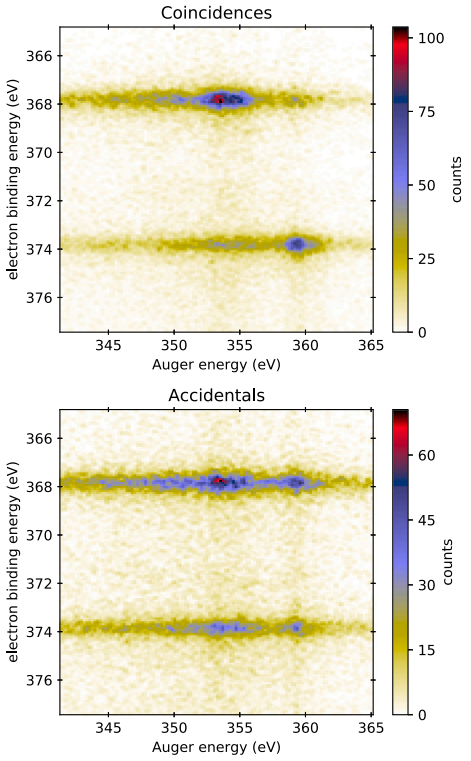

Fig. 3. Raw data maps (2D-histograms): *(top)* All coincidences acquired from single pulses. *(bottom)* Accidentals recorded for two consecutive pulses. The energy of the Auger electron is plotted on the x-axis and the binding energy of the photoelectron is shown on the y-axis.

In contrast to their setup, like many other coincidence setups nowadays, the CoESCA station can record a coincidence map and a corresponding map of accidental coincidences in one run, without changing the analyser settings or any other experimental parameter. The best guess of the true coincidences dataset is derived in post-processing by a simple subtraction, see Eq. (2). For electron–electron coincidences from surfaces, the successful subtraction of the accidental coincidences contribution from the coincidence dataset has previously been demonstrated in [17].

For the measurements presented in this paper, we chose a photon energy of 700 eV and operated the beamline at a resolution of 100 meV. The ArTOF 10k spectrometer was set to record the Auger spectrum in the range of 335–359 eV kinetic energy, while the ArTOF 2 EW spectrometer was set to record the photoelectron spectra in the range of 318–330 eV kinetic energy. The total experimental resolution was around 0.6 eV, determined from fitting the PES lines. The position of the Fermi edge was used to calibrate the energy axis for both spectrometers in post-processing. The silver single crystal sample, Ag(111) (99.999%, MaTeK GmbH), was cleaned by repeated Ar^+ sputtering and annealing cycles until no signs of contamination of the Ag surface by other materials, especially carbon, nitrogen and oxygen were visible in the photoelectron spectra.

The photon flux was adjusted via the exit slit of the beamline to achieve singles count rates of 0.8×10^3 s^{-1} for the Auger region and 1.0×10^3 s^{-1} for the core level region. The total acquisition time was 24 h, which yielded 106124 coincidence counts from single pulses and 101504 accidental coincidence counts from cross-comparing two consecutive pulses, resulting in 55372 true coincident counts. This corresponds to a measured coincidence rate of $\nu_c = 1.2$ s^{-1}, composed of $\nu_t = 0.64$ s^{-1} true and $\nu_a = 0.59$ s^{-1} accidental coincidences and accidental-to-true ratio of $\nu_a/\nu_t = 0.92$. The photon pulse repetition rate was 1.25 MHz.

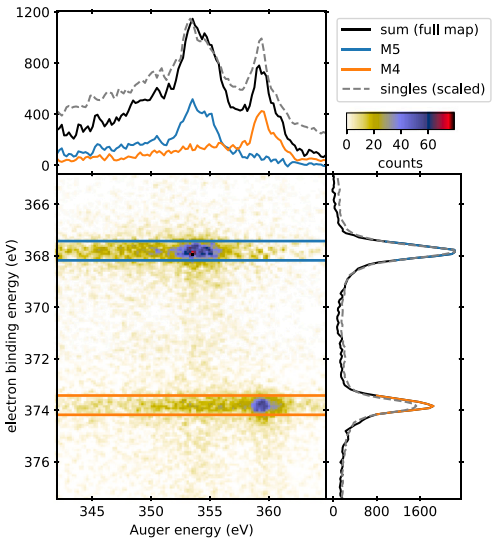

Fig. 4. True coincidence map derived from the raw data shown in Fig. 3, see text for more details on how the true map is obtained. Coloured frames in the map indicate the integration regions for the Auger spectra in coincidence with the M_4 ($3d_{3/2}$, orange) or the M_5 ($3d_{5/2}$, blue), respectively. On the left are the integrated photoelectron spectra and the Auger spectra are plotted on top of the map. In addition, the sum of the true map (black) and the non-coincident singles spectra (grey, dashed) derived from the accidentals map are shown. The M_5NN Auger spectrum is an intrinsic spectrum already, while the M_4NN spectrum still contains up to 6% of true coincident background originating from scattered M_5 photoelectrons. See text and Fig. 5 for a description of the origin of this background and an estimated intrinsic M_4NN Auger spectrum.

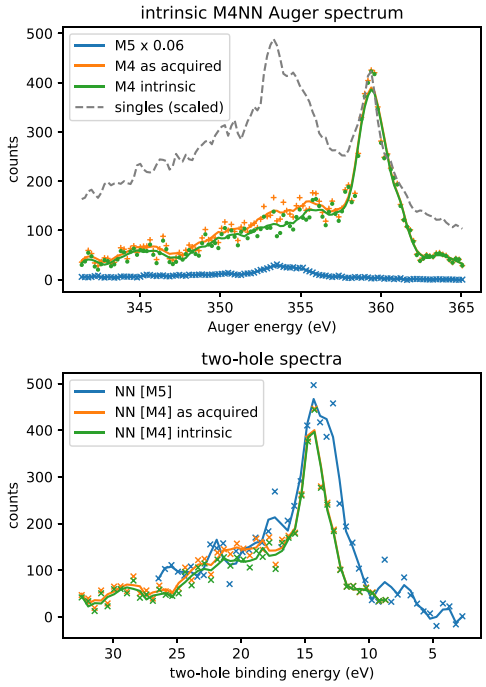

Fig. 5. *(top)* Measured M_4VV coincidence spectrum (orange), scaled M_5NN coincidence spectrum (blue) and their difference as best guess for the intrinsic M_4NN spectrum (green, see text for details). *(bottom)* Two-hole binding energy spectra: Comparison of M_5NN (blue), M_4NN as measured (orange) and derived intrinsic M_4NN (green). The markers in both plots are the measured data. The solid lines are the data smoothed with a Savitzky–Golay filter [20] as guide for the eye.

We were operating the ArTOF 2 EW analyser at its design limits and therefore, the transmission function along its energy window was not constant. For the present analysis, it is sufficient to account for this in post-processing by correcting the spectral intensities with a linear transmission function such, that for the singles photoelectron spectra (PES) the ratio of M_5 peak area over M_4 peak area would match the literature value of 0.67 [18]. In a recent study, the potential to operate angular resolved time of flight spectrometers beyond the standard limits and extending the time of flight range which can be analysed has been shown [19]. The ArTOF 10k detector, used for measuring the Auger spectra, was operated well within its specifications, with a constant transmission function.

The data maps as acquired are shown in Fig. 3. Fig. 4 shows the true coincidence map.

The coloured frames in the map mark the integration regions, used for extracting the Auger spectra obtained in coincidence with the $3d_{3/2}$ (orange) and $3d_{5/2}$ (blue) photoelectron peaks, respectively. These are plotted on top together with the full sum of the coincidence map. Also the singles spectrum is shown. It is clearly seen that the singles spectrum has a much larger background. This reduction of background is another advantage of recording the Auger spectrum in coincidence with the appropriate photoelectron region. The PES spectra are plotted on the right. The PES peaks have two equivalent denotations: $3d_{3/2}$ or M_4 for the peak at $E_b = 373.8$ eV and $3d_{5/2}$ or M_5 for the peak at $E_b = 367.8$ eV.

The spectrum obtained in coincidence with the $3d_{5/2}$ photoelectron line is a pure M_5NN Auger spectrum. For the spectrum in coincidence with the $3d_{3/2}$ photoelectron line the situation is, however, slightly different. The orange region in the coincidence map contains not only $3d_{3/2}$ photoelectrons. There is also a contribution from $3d_{5/2}$ photoelectrons, which have lost energy due to shake-up or inelastic loss processes. n the case of silver these additional excitations will be delocalised and will not significantly modify the $3d_{5/2}$ decay spectrum. For this reason the spectrum obtained by integration of the orange region will contain a contribution which is identical to the M_5NN Auger spectrum. In order to estimate the intensity of this contribution we have made a numerical fit of the 3d photoelectron peaks. As a model for the inelastic tail of the spectra we have used a Shirley background. From the fit we can then determine the intensity of the tail of the $3d_{5/2}$ spectrum in the integration region of the $3d_{3/2}$ peak. We find that, for our experiment, this contribution amounts to about 6% of the M_4 peak intensity and we use this as an upper limit for the M_5NN contribution to the M_4NN spectrum. Note, that the amount of this type of true coincident noise depends on the amount of inelastic scattered signal in the recorded true coincident spectrum and thus on the full width of the detection window in energy space. Therefore our value of 6% is true only for this experiment. Another source for such a contribution to the coincidence background could be due to a Coster–Kronig (CK) type decay. For silver, however, only M_4M_5O CK are energetically allowed, and the cross-sections for those are negligibly small.

The M_4NN spectrum is shown in the top panel of Fig. 5 before and after correction for the M_5NN contribution. It is clearly seen that the M_5NN contribution background is present on the low kinetic energy side of the main peak. The main M_4NN peak is therefore unaffected by the M_5 contribution, as a result of the good resolution of the CoESCA setup. The correction is also very small and changes the appearance of the spectrum very little. Also the fraction of M_5 contribution depends on the resolution of the setup. If measured with lower resolution the relative amount of the M_5 contribution would be larger.

The bottom panel of Fig. 5 shows the measured and intrinsic M_4 and M_5 two-hole spectra. These were obtained by summing the kinetic energies for the true coincidences, as described in the previous section. The data was then sorted in a histogram with equidistant bins of 500 meV.

5. Summary & outlook

The APECS technique has been introduced and a detailed overview of previous experiments on this topic was given. The experimental end

station for APECS at the BESSY II synchrotron facility, the CoESCA station, has been described together with important basic considerations on the data acquisition and treatment procedure in an electron–electron coincidence experiment. Fundamental limits on acquisition times and Signal-to-Noise ratio have been derived. We have presented the first APECS results using the CoESCA station on a clean Ag(111) single crystal for measuring coincidences between the Ag 3d core levels (M_4 and M_5) and the corresponding Auger electrons from $M_{45}NN$ Auger decays. The acquired true coincidence spectrum for the M_5NN Auger decay is already intrinsic. The acquired M_4NN Auger spectrum, however, still contains contributions from the M_5NN decay. We have explained the origin of these contributions and presented a method to obtain an estimate of the clean, intrinsic M_4NN spectrum. Furthermore, we extracted two-hole binding energy spectra for each Auger decay, M_4NN and M_5NN, respectively, from the true coincidences map. These spectra can be determined only from coincidence measurements and show the distribution of the total energy needed to create a coincident Auger electron–Photoelectron pair, leaving two holes in the sample's electronic system.

Further recent results from the CoESCA station on Auger- and Photoelectron coincidences of molecular O_2 adsorbed on Ag(111) [21] and quantifying Ni $L_{2,3}$ core-hole relaxation pathways [22] have been submitted for publication.

In principle, the CoESCA station could handle at least up to 5 MHz pulses repetition rate, i.e. 4 times the present value, yielding 4 times shorter acquisition times for the same data quality. Recent developments on the BESSY machine side give hope to achieve these higher pulse repetition rates in the near future. They are developing a TRIBs mode of operation for the storage ring [23,24], where a selected number of the electron bunches is pushed to an alternative orbit. This alternative orbit could be filled with a 5 MHz fill pattern and the light pulses originating from it can be separated in the beamlines.

Declaration of competing interest

The authors declare that they have no known competing financial interests or personal relationships that could have appeared to influence the work reported in this paper.

Acknowledgements

This work has been supported by the European Research Council (FP7/2007-2013)/ERC grant agreement no. [321319], the Swedish Research Council and Carl Tryggers Foundation for Scientific research (CTS), Sweden.

References

[1] H.W. Haak, G.A. Sawatzky, T.D. Thomas, Auger-photoelectron coincidence measurements in copper, Phys. Rev. Lett. 41 (26) (1978) 1825.

[2] C.P. Lund, S.M. Thurgate, A.B. Wedding, Auger photoelectron coincidence spectroscopy studies: Trends in the L 2, 3-M 4, 5 M 4, 5 line shapes across the 3D transition-metal series, Phys. Rev. B 55 (8) (1997) 5455.

[3] T. Kakiuchi, E. Kobayashi, N. Okada, K. Oyamada, M. Okusawa, K.K. Okudaira, K. Mase, Development of an electron electron ion coincidence analyzer for Auger photoelectron coincidence spectroscopy (APECS) and electron ion coincidence (EICO) spectroscopy, J. Electron Spectrosc. Relat. Phenom. 161 (1–3) (2007) 164–171.

[4] T. Kakiuchi, M. Tahara, S. Hashimoto, N. Fujita, M. Tanaka, K. Mase, S.-i. Nagaoka, Surface-site-selective study of valence electronic states of a clean Si (111)-7× 7 surface using Si L 23 VV Auger electron and Si 2 p photoelectron coincidence measurements, Phys. Rev. B 83 (3) (2011) 035320.

[5] T. Kakiuchi, N. Fujita, K. Mase, M. Tanaka, Study of local valence electronic states of SiO_2 ultrathin films grown on Si (111) by using auger photoelectron coincidence spectroscopy: Upward shift of valence-band maximum depending on the interface structure, J. Phys. Soc. Japan 81 (7) (2012) 074706.

[6] S. Svensson, N. Mårtensson, E. Basilier, P.A. Malmquist, U. Gelius, K. Siegbahn, Lifetime broadening and CI-resonances observed in ESCA, Phys. Scr. 14 (4) (1976) 141–147, http://dx.doi.org/10.1088/0031-8949/14/4/004.

[7] I. Kostanovskiy, F.O. Schumann, Y. Aliaev, Z. Wei, J. Kirschner, Core-resonant double photoemission from palladium films, J. Phys.: Condens. Matter 28 (1) (2015) 015601, http://dx.doi.org/10.1088/0953-8984/28/1/015601.

[8] Z. Wei, F.O. Schumann, C.H. Li, L. Behnke, G. Di Filippo, G. Stefani, J. Kirschner, Dynamic screening probed by core-resonant double photoemission from surfaces, Phys. Rev. Lett. 113 (2014) 267603, http://dx.doi.org/10.1103/PhysRevLett.113.267603, URL https://link.aps.org/doi/10.1103/PhysRevLett.113.267603.

[9] F.O. Schumann, J. Kirschner, J. Berakdar, Mapping out electron-electron interactions at surfaces, Phys. Rev. Lett. 95 (11) (2005) 117601.

[10] F.O. Schumann, C. Winkler, G. Kerherve, J. Kirschner, Mapping the electron correlation in two-electron photoemission, Phys. Rev. B 73 (4) (2006) 041404.

[11] Webpage, The CoESCA station at UE52-PGM beamline at BESSY II, Berlin, 2019, URL https://tinyurl.com/uvq4j53.

[12] D.R. Batchelor, T. Schmidt, R. Follath, C. Jung, R. Fink, M. Knupfer, A. Schöll, T. Noll, F. Siewert, B. Büchner, E. Umbach, An energy-dispersive VUV beamline for NEXAFS and other CFS/CIS studies, Nucl. Instrum. Methods Phys. Res. A 575 (3) (2007) 470–475, http://dx.doi.org/10.1016/j.nima.2007.02.108.

[13] R. Ovsyannikov, P. Karlsson, M. Lundqvist, C. Lupulescu, W. Eberhardt, A. Föhlisch, S. Svensson, N. Mårtensson, Principles and operation of a new type of electron spectrometer–ArTOF, J. Electron Spectrosc. Relat. Phenom. 191 (2013) 92–103.

[14] K. Holldack, R. Ovsyannikov, P. Kuske, R. Müller, A. Schälicke, M. Scheer, M. Gorgoi, D. Kuehn, T. Leitner, S. Svensson, N. Mårtensson, A. Föhlisch, Single bunch X-ray pulses on demand from a multi-bunch synchrotron radiation source, Nature Commun. 5 (1) (2014) http://dx.doi.org/10.1038/ncomms5010.

[15] E. Jensen, R.A. Bartynski, S.L. Hulbert, E.D. Johnson, Auger photoelectron coincidence spectroscopy using synchrotron radiation, Rev. Sci. Instrum. 63 (1992) 3013.

[16] D.A. Arena, R.A. Bartynski, S.L. Hulbert, A method for determining intrinsic shapes of overlapping spectral lines in auger-photoelectron coincidence spectroscopy, Rev. Sci. Instrum. 71 (4) (2000) 1781–1787.

[17] F.O. Schumann, R.S. Dhaka, G.A. van Riessen, Z. Wei, J. Kirschner, Surface state and resonance effects in electron-pair emission from Cu(111), Phys. Rev. B 84 (2011) 125106, http://dx.doi.org/10.1103/PhysRevB.84.125106, URL https://link.aps.org/doi/10.1103/PhysRevB.84.125106.

[18] N. Mårtensson, R. Nyholm, Electron spectroscopic determinations of m and n core-hole lifetimes for the elements Nb—Te ($Z = 41 - 52$), Phys. Rev. B 24 (1981) 7121–7134, http://dx.doi.org/10.1103/PhysRevB.24.7121, URL https://link.aps.org/doi/10.1103/PhysRevB.24.7121.

[19] M. Huth, A. Trützschler, C.-T. Chiang, R. Kamrla, F.O. Schumann, W. Widdra, Extended energy range analysis for angle-resolved time-of-flight photoelectron spectroscopy, J. Appl. Phys. 124 (16) (2018) 164504, http://dx.doi.org/10.1063/1.5048515, arXiv:https://doi.org/10.1063/1.5048515.

[20] A. Savitzky, M.J.E. Golay, Smoothing and differentiation of data by simplified least squares procedures, Anal. Chem. 36 (8) (1964) 1627–1639.

[21] F.O.L. Johansson, T. Leitner, I. Bidermane, A. Born, A. Föhlisch, S. Svensson, N. Mårtensson, A. Lindblad, Auger- and photoelectron coincidences of molecular O_2 adsorbed on Ag(111), J. Electron Spectrosc. Relat. Phenom. (2020) submitted for publication.

[22] A. Born, T. Leitner, I. Bidermane, R. Ovsyannikov, S. Svensson, N. Mårtensson, A. Föhlisch, Quantification of Ni $L_{2,3}$ core-hole relaxation pathways utilizing auger photoelectron coincidence spectroscopy, Phys. Rev. B 103 (2021) 115121, http://dx.doi.org/10.1103/PhysRevB.103.115121.

[23] M. Ries, et al., Transverse resonance Island buckets at the MLS and BESSY II, in: Proc. 6th International Particle Accelerator Conference, IPAC'15, Richmond, VA, USA, May 3-8, 2015, in: International Particle Accelerator Conference, (6) JACoW, Geneva, Switzerland, 2015, pp. 138–140, http://dx.doi.org/10.18429/JACoW-IPAC2015-MOPWA021, URL http://jacow.org/ipac2015/papers/mopwa021.pdf.

[24] P. Goslawski, et al., Two orbit operation at bessy II - During a user test week, in: 10th International Particle Accelerator Conference, 2019, p. THYYPLM2, http://dx.doi.org/10.18429/JACoW-IPAC2019-THYYPLM2.